

# Integrated microelectronic device for label-free nucleic acid amplification and detection†

Chih-Sheng Johnson Hou,<sup>a</sup> Michel Godin,<sup>b</sup> Kristofor Payer,<sup>c</sup> Raj Chakrabarti<sup>df</sup> and Scott R. Manalis<sup>\*be</sup>

Received 22nd November 2006, Accepted 18th January 2007

First published as an Advance Article on the web 8th February 2007

DOI: 10.1039/b617082j

We present an integrated microelectronic device for amplification and label-free detection of nucleic acids. Amplification by polymerase chain reaction (PCR) is achieved with on-chip metal resistive heaters, temperature sensors, and microfluidic valves. We demonstrate a rapid thermocycling with rates of up to 50 °C s<sup>-1</sup> and a PCR product yield equivalent to that of a bench-top system. Amplicons within the PCR product are detected by their intrinsic charge with a silicon field-effect sensor. Similar to existing optical approaches with intercalators such as SYBR Green, our sensing approach can directly detect standard double-stranded PCR product, while in contrast, our sensor does not require labeling reagents. By combining amplification and detection on the same device, we show that the presence or absence of a particular DNA sequence can be determined by converting the analog surface potential output of the field-effect sensor to a simple digital true/false readout.

## Introduction

The extraordinarily high sensitivity, large dynamic range and reproducibility of the polymerase chain reaction (PCR) have made it one of the most widely used techniques for analyzing nucleic acids.<sup>1,2</sup> As a result, considerable effort has been directed towards developing miniaturized and integrated systems for PCR. Examples include the inclusion of capillary gel electrophoresis, microvalves and pumps, hybridization chambers, and sample purification stages.<sup>3–6</sup> Not only is integration advantageous in terms of efficient sample handling and automation, scaling down PCR itself leads to many improvements including increased thermal response rate, more uniform temperature distribution, reduced reagent consumption, and in a number of instances, more reproducible performance in single molecule PCR.<sup>7–9</sup> Given these merits, several commercial prototypes have been developed that perform favorably in real-world settings.<sup>10–12</sup>

While there have been extensive advances in miniaturized PCR systems, progress on integrated microfabricated readout mechanisms have been rather limited, and most systems rely on off-chip optical detection modules to measure the final product.<sup>13</sup> Existing optical detection platforms typically

include CCD cameras, photodiodes, and photomultiplier tubes.<sup>11,12,14–16</sup> While such hardware has adequate sensitivity for detecting PCR product in sample volumes significantly lower than that of bench-top systems, most are difficult to miniaturize and integrate into a compact analytical system. For example, some portable systems incorporating external LEDs and photodetectors weigh between 1 kg and 4 kg each.<sup>17–19</sup> To address these limitations, several groups have successfully embedded photodetectors within integrated PCR platforms.<sup>5,20,21</sup> However, these devices still rely on external excitation sources.

Optical detection of nucleic acids in miniaturized systems is also challenging because the signal originates from dye molecules in solution, and thus the strength of the signal scales with sample volume. Therefore, there is a direct conflict between the goals of obtaining a strong optical signal and reducing reagent consumption in the microfluidic system. Furthermore, optical readout requires that PCR product markers such as Sybr Green and Taqman probes be added to the reagents, and this can induce inhibitory effects on PCR or require extensive effort to optimize.<sup>22–24</sup>

Field-effect sensors, whose electronic properties are modulated by changes in surface potential, have been implemented using various micro- and nano-fabrication techniques for label-free sensing of charged molecules such as nucleic acids.<sup>25–29</sup> While the detection has typically been performed in a buffer containing only DNA, we have recently demonstrated that field-effect sensors can quantify the product in an unprocessed PCR mixture.<sup>30</sup> In this paper, we present a microdevice that integrates thermocycling with a silicon field-effect platform for label-free PCR detection. The integrated thermocycler achieves a ramp rate of up to 50 °C s<sup>-1</sup> and the resulting PCR product yield is comparable to benchtop systems. We demonstrate that a polycation modified field-effect sensor surface is primarily sensitive to the total mass of double-stranded PCR product in the relevant mass concentration range from 3.2 ng μL<sup>-1</sup> to

<sup>a</sup>Department of Electrical Engineering and Computer Science, Massachusetts Institute of Technology, Cambridge, MA 02139, USA

<sup>b</sup>Department of Biological Engineering, Massachusetts Institute of Technology, Cambridge, MA 02139, USA  
E-mail: scottm@media.mit.edu

<sup>c</sup>Microsystems Technology Laboratories, Massachusetts Institute of Technology, Cambridge, MA 02139, USA

<sup>d</sup>Department of Chemistry, Massachusetts Institute of Technology, Cambridge, MA 02139, USA

<sup>e</sup>Department of Mechanical Engineering, Massachusetts Institute of Technology, Cambridge, MA 02139, USA

<sup>f</sup>Department of Chemistry, Columbia University, New York, NY 10025, USA

† The HTML version of this article has been enhanced with colour images.

100 ng  $\mu\text{L}^{-1}$ , but not to other higher-concentration components in the PCR mixture. By combining amplification and detection on the same device, we show that the presence or absence of the HIV-I GAG gene sequence can be determined by converting the analog surface potential output to a simple digital true/false readout.

## Experimental

### Field-effect sensor fabrication

A process using mostly CMOS-compatible tools was developed to fabricate electrolyte-insulator-semiconductor (EIS) field-effect sensors on planar silicon substrates.<sup>30</sup> First, 20 nm silicon oxide was thermally grown on 6" n-type (phosphorus doped) 20–50  $\Omega$  cm silicon substrates to form a protective layer against surface sputtering. Ion implantation of active sensor areas (lightly-doped p-type), conductive traces (heavily-doped p-type), and an insulating ground plane (heavily-doped n-type) was then carried out in sequence using photoresist implant masks. Annealing of the substrate at 1050 °C was performed to activate and drive in the dopants, forming 800 nm deep sensing regions. An insulating layer of 800 nm silicon-rich nitride and 100 nm PECVD oxide was deposited for both electrical insulation as well as compatibility with the PCR reaction.<sup>31</sup> Metal contact holes and 80  $\times$  80  $\mu\text{m}^2$  sensor areas were then etched in the dielectric layer in a single step. Finally, 30 nm Cr and 1  $\mu\text{m}$  Au were evaporated on the substrate and patterned as conductive traces using a liftoff process. With the exception of ion implantation steps, the silicon processing was accomplished at the Massachusetts Institute of Technology Microsystems Technology Laboratory.

### Microfluidics fabrication and encapsulation

Microfluidic channels and integrated valves were fabricated using a multilayer soft lithography molding technique.<sup>32</sup> The valve mold was patterned out of a 60  $\mu\text{m}$  SU-8 50 negative resist (MicroChem, Newton, MA). The fluidic mold was fabricated from a combination of positive AZP4620 photoresist (Clariant, Somerville, NJ) and SU-8 50 (MicroChem). Patterns defining channels under the valve areas were first fabricated by patterning a layer of 15  $\mu\text{m}$  AZP4620, and subsequently hard-baking the wafer at 200 °C for 20 min to reflow the resist so the cross section became rounded. A 75  $\mu\text{m}$  layer of SU-8 50 was then spun onto the same wafer, and a photomask was aligned to features defined by the positive resist to define fluid channels with a rectangular cross section. Both molds were silanized by exposure to (tridecafluoro-1,1,2,2-tetrahydrooctyl)-1-trichlorosilane vapor (United Chemical Technologies, Bristol, PA) for 1 h. To fabricate the elastomeric structure for microfluidics and valves, 80 g of 7 part A : 1 part B RTV (General Electric, Wilton, CT) was cast over the valve mold and baked at 80 °C for 20 min. The partially cured elastomer was peeled off the mold and access holes were punched with a 19 gauge needle. 20 part A : 1 part B RTV was spin-coated on the fluidic master at 1100 rpm for 40 s, and baked in the oven at 80 °C for 15 min. The partially cured valve layer was then aligned and bonded to the fluidic layer and baked overnight. The bonded devices were then

peeled off the fluidic master, and access ports to the fluid channels were then drilled. To assemble the silicon and elastomer layers, the silicon and elastomer substrates were first rinsed with ethanol. The surfaces to be bonded were exposed to air plasma for 20 s in a Harrick PDC-32G RF plasma cleaner (Harrick Plasma, Ithaca, NY), and finally the two pieces were aligned and bonded shortly after plasma treatment. The final device was left in air for 10 min before use to strengthen the elastomer–silicon bond. The total volume of the microchannel is approximately 2  $\mu\text{L}$ .

### Surface potential measurements

The measurement method has been previously reported in detail.<sup>33</sup> Briefly, a 4 kHz, 50 mV<sub>pp</sub> AC voltage was delivered to the on-chip gold signal electrode shown in Fig. 1b. The resulting alternating current through the field-effect sensor was amplified and converted by a lock-in amplifier to a dc voltage.

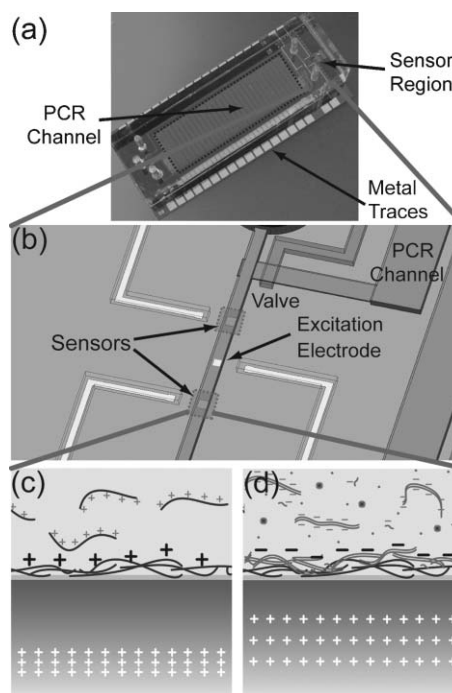


**Fig. 1** Device layout and concept. (a) Photograph of an integrated device with embedded sensors (right dotted area), PCR microfluidic channel with integrated valves (left dotted area), and metal resistive heaters and temperature sensors (features above and below PCR channel). (b) 3D rendering of device centered on sensors (top and bottom squares) and excitation metal electrode. Adjacent features include gold traces for electrical connections, inlet of sensor channel, and an integrated valve controlling the interface to the PCR channel. The gold traces are connected to the respective gold electrode and field-effect sensors by buried conductive traces in silicon (not shown). Conceptual schematic of sensor cross section illustrating the physical changes caused by binding of (c) positively charged polyelectrolyte followed by (d) negatively charged product DNA in a PCR mix. The mobile positive charge carriers in the sensor redistribute depending on the polarity of surface charge, affecting the depth of the charge depletion region in the process. This subsequent change in depletion capacitance is monitored by applying an AC voltage to the metal electrode and measuring the resulting current through the doped sensor region in silicon.

Before an experiment, the bias potential applied to the sensor was set at a level where the slope and linearity of the output vs. sensor bias voltage curve are maximized. The relative surface potential response of the sensor as a function of the lock-in amplifier output was calibrated by applying a 2.5 mV bias step to the sensor. All surface potential values reported in this paper are relative.

### Temperature controller

On-chip and off-chip temperature control has been implemented. For on-chip temperature sensing, a 100  $\mu\text{A}$  current was passed through a set of gold traces surrounding the PCR channels (Fig. 1a) and the voltage drop across the traces was measured. The devices were placed in a convection oven to derive the resistance vs. temperature calibration data. Custom software implementing on-off control algorithm was used to control the amount of power supplied to the heater resistive traces in feedback with temperature readings. A custom circuit board was made to control solenoid valves (Lee Company, Westbrook, CT) to blow 15 psi compressed air on the backside of the device to accelerate cooling. Off-chip temperature control was achieved using a thermoelectric module (mounted against the chip) powered by a pulse-width-modulated PID controller (model 5C7-378, McShane Inc., Medina, Ohio). A custom Labview program was implemented for thermocycling applications. To test the temperature uniformity of the device, dilutions of thermochromic crystal (R90C5W, Hallcrest, Glenview, IL) were loaded into the microfluidic channels and imaged. Electronic measurements were performed at 28  $^{\circ}\text{C}$ .

### Polymerase chain reaction protocol

Forward primer, 5' ATC AAG CAG CCA TGC AAA TG 3', and reverse primer, 5' CCT TTG GTC CTT GTC TTA TGT C 3', were used to amplify a 291 base pair (bp) fragment of the HIV-I GAG gene (Genebank accession no. K02007). The PCR buffer consisted of 10 mM Tris-HCl (pH 8.3), 20 mM KCl, and 2 mM  $\text{MgCl}_2$ . The reaction mixture included the PCR buffer, 0.1 mM each of four dNTPs, 0.4  $\mu\text{M}$  each of forward and reverse primers, 5 U Taq polymerase (New England BioLabs, Ipswich, MA), 0.1% *n*-dodecyl  $\beta$ -D-maltoside (DDM, Sigma, St. Louis, MO), and 0.1 ng  $\mu\text{L}^{-1}$  control template. The positive control template was a 4.5 kbp clone vector plasmid containing a segment of the HIV-I GAG gene (Maxim Biotech, Rockville, MD), and the negative control template was  $\Phi\text{X174}$  Virion DNA (New England BioLabs). The PCR was performed for 25 cycles of 90  $^{\circ}\text{C}$  for 15 s, 52  $^{\circ}\text{C}$  for 15 s, and 68  $^{\circ}\text{C}$  for 30 s in a micro-device, or 91  $^{\circ}\text{C}$  for 20 s, 52  $^{\circ}\text{C}$  for 35 s, and 68  $^{\circ}\text{C}$  for 40 s in a commercial thermocycler (Opticon DNA Engine, MJ Research, Waltham, MA). During thermocycling, the AC voltage applied to the temperature controller was switched off. The products were visualized with Sybr Safe Gel kits (Invitrogen, Carlsbad, CA) and quantitated using DNA 12000 Labchip kits (Agilent, Palo Alto, CA).

### Microfluidic system operations

The PCR channel was first treated with deionized water containing 0.1% DDM for 10 min. Buffered oxide etchant

(7 : 1  $\text{H}_2\text{O}$  : HF) was introduced into the sensor channel for 20 s, and immediately flushed with PCR buffer afterwards. The sensor was equilibrated in a constant flow of PCR buffer for 2 h, a process which regenerated native oxide on the sensor surface. The inlet of the sensor channel was connected to a sample selection valve (Upchurch Scientific, Oak Harbor, WA), which in turn was connected to vials containing PCR buffer and 0.2  $\mu\text{g}$   $\mu\text{L}^{-1}$  poly-L-lysine hydrobromide (PLL, MW 15 000–30 000, Sigma). For sensor characterization experiments, vials containing dNTP, 50 bp DNA ladder (New England BioLabs), 1 kb DNA ladder (New England BioLabs), and primers diluted to various concentrations with PCR buffer were also used. A 6 psi pressure was applied to the selected vial using a syringe needle inserted into the cap of the vial, and in standby mode a constant flow of PCR buffer was maintained through the sensor. Before every measurement step, the sensor was functionalized by flowing PLL over the sensor for 3 min followed by a 2 min rinse with PCR buffer to wash away unbound PLL and achieve a steady baseline signal. To analyze the content inside the PCR channel, the pressure at the external selection valve was turned off, and the initially closed on-chip valves isolating the PCR and sensor channels were released. A 3 psi pressure was applied at the inlet of the PCR channel for 3 min to transfer the content of the PCR channel over the sensor, after which the on-chip valves were closed and the main buffer flow through the selection valve at 6 psi was restored. The signals were recorded at a sampling rate of 10 Hz.

## Results and discussion

### Device architecture

Devices were fabricated using techniques of both semiconductor processing for electronic DNA sensing and multilayer soft-lithography<sup>32</sup> for integrated microfluidic control. Fig. 1a shows a top view photo of the device and Fig. 1b shows a 3D rendering of the microfluidic channel containing a pair of field-effect sensors. The device consists of two subunits (field-effect sensors and PCR thermocycler) that are independently functional. The device is designed to carry out end-point detection of the PCR product: the sample is thermocycled in the PCR channel which is isolated by on-chip valves, and at the same time the electronic sensor is functionalized with a polycation solution of poly-L-lysine (PLL). The positively charged sensor surface (Fig. 1c) gives it the ability to capture the intrinsically negatively charged DNA generated by PCR (Fig. 1d), which is delivered from the PCR microchannels to the microelectronic sensor as outlined by Fig. 2. The binding of charged molecules such as PLL or DNA affects the distribution of extrinsic mobile charge carriers, and this is measured by monitoring the capacitance of the depletion region near the sensor surface.<sup>34</sup>

### Microchip PCR

The device integrates all the components required to perform temporal thermocycling. After the PCR microchannel is filled with reagents, on-chip valves are shut to prevent sample evaporation, and on-chip temperature sensors and heaters

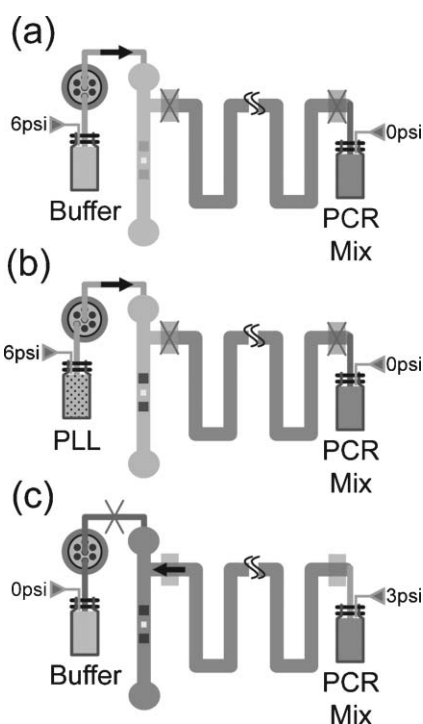


**Fig. 2** Microfluidic operation for sensor functionalization and detection using a combination of on-chip and external selection valves. (a) PCR measurement buffer is injected through an external selection valve during sensor stand-by mode. (b) Injection of PLL from a different vial by switching the external selection valve to functionalize the sensor for DNA detection. (c) Valves isolating sensor channels from the PCR channel are opened to enable measurement of PCR product amplified on chip. After step (b) or (c), sensor rinsing by step (a) is necessary to wash away unbound molecules.

cycle the temperature of the microdevice to carry out the amplification reaction. Temperature is determined by measuring the resistance of gold traces on the chip which varies linearly with respect to temperature. Due to the low thermal mass of the microdevice, the on-chip heaters, together with forced convective cooling by compressed air, heat and cool at approximately  $50\text{ }^{\circ}\text{C s}^{-1}$  (Fig. 3a). The low noise and linearity of the metal sensing traces enables the on/off temperature controller to achieve a resolution of  $0.1\text{ }^{\circ}\text{C}$  and a stability of  $0.3\text{ }^{\circ}\text{C}$ . To verify the temperature uniformity of the PCR channel as well as the accuracy of temperature sensor calibration, thermochromic liquid crystals with  $1\text{ }^{\circ}\text{C}$  red-bandwidth at  $90\text{ }^{\circ}\text{C}$  was injected to the PCR channels. While heat generation is concentrated over a small area on the chip (Fig. 1a), the high thermal conductivity of silicon enables uniform temperature distribution throughout the device. For comparison, an off-chip temperature controller setup based on an off-chip thermoelectric stage and PID control has also been implemented. Although the temperature ramp rate is slower than that of the integrated heaters, the off-chip configuration eliminates the need to recalibrate the temperature sensing traces for each new device that is used.

Since microchannels have a high surface-to-volume ratio, the channel surface properties are one of the most critical determinants of PCR product yield. Two major categories of

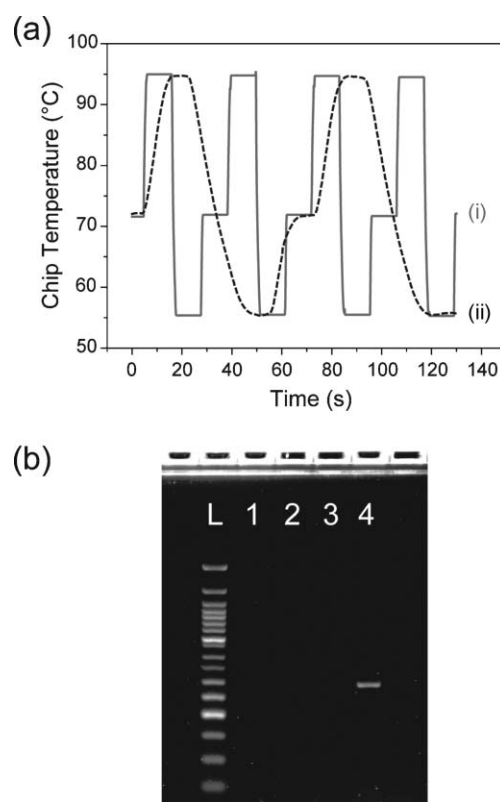


**Fig. 3** Microfabricated thermocycler performances. (a) Thermal performance comparison of on-chip and off-chip thermocycling configurations. Identical thermocycling protocol of  $95\text{ }^{\circ}\text{C}$  for 10 s,  $55\text{ }^{\circ}\text{C}$  for 10 s, and  $72\text{ }^{\circ}\text{C}$  for 10 s was carried out using integrated metal resistive heater and temperature sensors with compressed air cooling, solid trace (i), and an external thermoelectric stage pressed against the backside of the device, dotted trace (ii). (b) Analysis of chip PCR product by gel electrophoresis. PCR reactions containing the primer set designed to amplify a 291 bp segment of HIV-I GAG gene were performed with two templates, one with and one without the gene. Lane L, 50 bp DNA ladder; lane 1, negative template before thermocycling; lane 2, positive template before thermocycling; lane 3, negative template after thermocycling; lane 4, positive template after thermocycling. The samples were displayed in Invitrogen 2% E-Gel with Sybr Safe dye.

surface passivation strategies for maximizing yield are: (i) static passivation where channels are pre-treated with coatings during device fabrication or immediately before PCR, and (ii) dynamic passivation where passivating chemicals are mixed directly in with the PCR solution.<sup>13</sup> Typical passivation coatings include silicon oxide surface modification for static passivation,<sup>35</sup> bovine serum albumin (BSA) for both passive and static passivation,<sup>7,18,36</sup> polyethylene glycol (PEG) for dynamic passivation,<sup>37,38</sup> and various channel silanizing agents for static passivation.<sup>16,39</sup> We have applied both static and dynamic passivation using a mild nonionic surfactant DDM;<sup>40</sup> after flushing the channel with deionized water containing 0.1% DDM for 10 min, PCR reagents mixed with 0.1% DDM were used for amplification within the microchannel. Using this strategy, a clear gel electrophoresis band was observed for on-chip PCR product using the HIV-I GAG positive control template (Fig. 3b). Furthermore, when quantified by Agilent

LabChip kits, product concentrations in excess of  $40 \text{ ng } \mu\text{L}^{-1}$  were measured for on-chip PCR products, compared to  $35 \text{ ng } \mu\text{L}^{-1}$  and above for identical reagents amplified in a bench-top system. When we carried out control experiments to test whether DDM would interfere with electronic multilayer-based PCR detection, no transient signal or permanent baseline shift was observed, indicating that the passivating agent is compatible with our sensing technique.

When conducting PCR with our device, we occasionally noticed that the PDMS valve would remain shut permanently after thermocycling, preventing any subsequent analysis of the PCR product. It is anticipated that more comprehensive PDMS surface treatments can alleviate these issues.<sup>41</sup>

### PCR sensor sensitivity characterization

The ability to measure the total amount of double-stranded DNA products present in an unprocessed PCR mixture would greatly simplify any detection protocol. Many hybridization-based approaches for nucleic acid detection,<sup>25,26,28,29,42</sup> which although provide additional amplicon sequence specificity in the case that an un-optimized PCR generates spurious products, requires additional steps or specialized asymmetric PCR protocols to generate single-stranded products.<sup>43,44</sup> We demonstrated the measurement of total double-stranded product concentration by using a polyelectrolyte capture surface that does not require additional sample processing after the PCR protocol.<sup>30</sup> Similar to optical approaches that use intercalators such as SYBR Green, the specificity of our detection format is entirely determined by the PCR protocol.

The sensing method is based on the electronic detection of layer-by-layer assembly of polyelectrolytes. First, the sensor surface is exposed to a solution containing positively charged polyelectrolytes PLL which bind to the negatively charged silicon oxide surface. This gives the sensor the ability to bind negatively charged DNA such as PCR product DNA. The adsorption of DNA to the PLL-coated surface reverses the polarity of the sensor surface, making it capable of binding a fresh layer of PLL. Alternating injections can be repeated indefinitely resulting in a polymeric multilayer of increasing thickness.<sup>45</sup> However, a cyclical pattern is observed in electronic output which is consistent with surface charge reversal: alternating depositions of positively charged polymer and negatively charged DNA onto the sensor surface results in decreases and increases in signal. Electronic detection of multilayer assembly has been performed for more than 20 deposited layers with no noticeable degradation in signal amplitude.<sup>25,27,30</sup> One noteworthy feature of the electronic multilayer assembly technique is that the response from a DNA injection is independent of the history of prior DNA injections, making the sensor amenable to blind sequential quantitation of unknown DNA samples.

For the sensor to be useful as a PCR detector, it must be capable of differentiating the double-stranded product from the other components of a PCR mix. We have previously shown that the electronic multilayer technique is sensitive primarily to double-stranded DNA product.<sup>30</sup> In contrast, dNTP and Taq polymerase produce transient signals during injection, which suggests that the association with the PLL

surface is weak. Furthermore, when template and primers are individually injected at PCR relevant concentrations, the response is significantly smaller than that from double-stranded DNA.

Developing PCR protocols for different targets inevitably involves varying the sizes and concentrations of the reagents and products. To demonstrate the generality of the sensing technique for different PCR conditions, this report provides further characterization of the sensors' response to nucleic acids of different lengths (including dNTP monomers) at a variety of mass concentrations. This provides a foundation for understanding how changing PCR parameters such as primer/dNTP concentrations, and/or final product concentrations can affect the sensor's response. Specifically, we have characterized the sensor response to dNTP, 20 bp ssDNA, 50 bp DNA ladder (50–1000 bp, weighted average length = 222 bp) and 1 kbp (500–10 000 bp, average length = 1491 bp) ladder, each at  $3.16 \text{ ng } \mu\text{L}^{-1}$ ,  $10 \text{ ng } \mu\text{L}^{-1}$ ,  $31.6 \text{ ng } \mu\text{L}^{-1}$ , and  $100 \text{ ng } \mu\text{L}^{-1}$ . The 50 bp ladder and 1 kbp ladder were chosen to represent the low and high ends of average diagnostic PCR product size ranges. This concentration range was selected to represent typical product concentrations between 20 and  $100 \text{ ng } \mu\text{L}^{-1}$  (as verified from various saturated PCR using Labchip kits). Typical primer concentrations of  $0.5 \text{ } \mu\text{M}$  each and dNTP concentrations of  $200 \text{ } \mu\text{M}$  each type of nucleotide<sup>46</sup> correspond to a mass concentration of approximately  $3 \text{ ng } \mu\text{L}^{-1}$  and  $100 \text{ ng } \mu\text{L}^{-1}$ , respectively.

Indeed, as shown in Fig. 4, the signal amplitudes correlate with both the length and concentrations of DNA. Injecting dNTP results in a transient response only (Fig. 4a). Even though the injection of DNA of different lengths caused a permanent response, as shown in Fig. 4b, the response to short 20 bp single-stranded oligonucleotide was weaker compared to those of longer double-stranded DNA ladders at the same mass concentrations. To demonstrate consistency among different devices,  $40 \text{ ng } \mu\text{L}^{-1}$  50 bp DNA ladder was injected during each experiment as a control, producing a change in surface potential of  $9.0 \pm 0.2 \text{ mV}$ . This variability is relatively small compared to the difference of greater than 8 mV observed between signals from short nucleotides and 50 bp ladders at  $100 \text{ ng } \mu\text{L}^{-1}$ . In contrast, the sensors responded very similarly to injections of 50 bp DNA ladder and 1 kbp DNA ladder at the same mass concentrations (Fig. 4b).

Several inferences can be drawn from the data. For relatively short DNA, the magnitude of the response correlates positively with length. However, as we obtained similar dose-response curves for 50 bp and 1 kbp DNA ladders, we conclude that for sufficiently long DNA, the response becomes independent of length and is instead dominated by the total nucleotide mass concentrations. Since PCR is a process that converts short oligomers and nucleotide monomers to longer double-stranded DNA, the measurements shown in Fig. 4 suggests that the magnitude of the sensor response can be used to determine whether or not the target sequence was amplified. This analysis also shows that when optimizing PCR protocols for sensitivity with field-effect readout, maximizing total product yield rather than product length should be the primary consideration. This property is desirable given that amplifying long templates can be very challenging.<sup>47</sup>

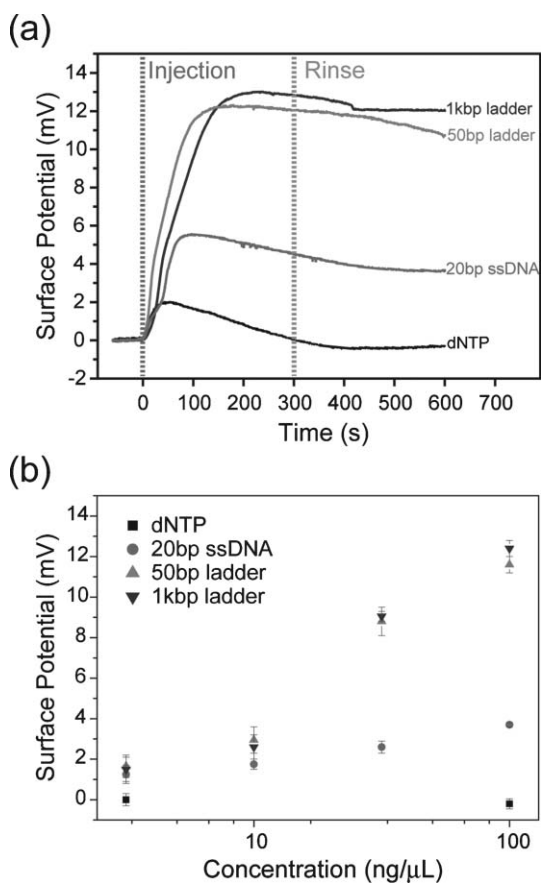


**Fig. 4** Characterization of sensor response to different DNA lengths. (a) Time-course measurement of surface potential of dNTP, 20 bp ssDNA, 50 bp dsDNA ladder, and 1 kbp dsDNA ladder at  $100 \text{ ng } \mu\text{L}^{-1}$ . Samples were injected for 5 min each (left dotted line) onto a surface coated with PLL, followed by rinsing with buffer (right dotted line). (b) PCR-relevant range of dose-response curve of nucleic acids of different sizes using the same injection protocols described in (a). Each series of curves was obtained from a unique device using an electronic polyelectrolyte multilayer detection technique. To ensure comparability between data, before the dose-response analysis, a control sample of 50 bp ladder at  $40 \text{ ng } \mu\text{L}^{-1}$  was measured, which yielded potential shifts  $9.0 \pm 0.2 \text{ mV}$ . Each data point is an average of two measurements  $\pm 1 \text{ SD}$ .

### Integrated PCR and label-free electronic sensing

Our device is configured to perform end-point detection of samples before and after on-chip thermocycling. The experimental protocol is as follows: (i) the sensor is first functionalized with PLL, (ii) as the PCR channel is filled with PCR reagents, a measurement is simultaneously acquired, (iii) once thermocycling is completed, the sensor is again functionalized with PLL, and (iv) the previously closed valves which isolated the PCR channel are opened and the content is delivered to the electronic sensor for a second measurement. Since each chip has two electronic sensors, a set of four curves is expected for each PCR experiment.

To demonstrate the utility of this protocol, two control experiments were performed using: (i) PCR mix which had a template containing HIV-I GAG gene and the primers designed to amplify a 291 segment in the template, and (ii)

PCR mix with the same conditions but with a virion template that did not contain the sequence. Fig. 5a and 5b show the time course surface potential data for measurements taken before and after thermocycling, respectively. In Fig. 5a, prior to thermocycling, there was a transient response during injection of the PCR sample but the sustained response after restoring the measurement buffer was all below 3.2 mV. This transient response was created not only by the presence of charged molecules (e.g. dNTPs) that caused temporary baseline shifts, but also by disturbance from the opening (and

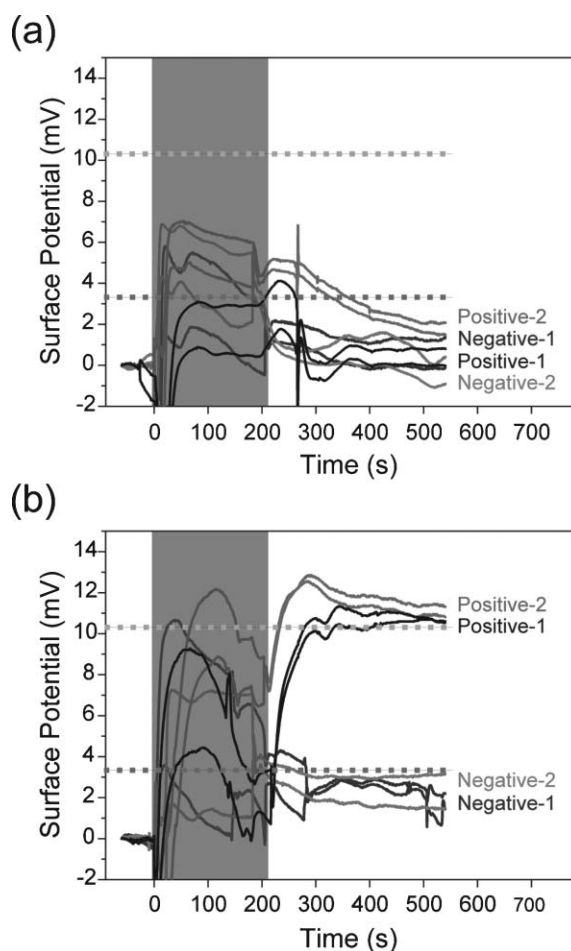


**Fig. 5** Integrated PCR and field-effect sensing of product. For each PCR experiment, measurements were taken both (a) before and (b) after thermocycling. Both negative and positive controls were carried out using the same PCR conditions for off-chip gel-electrophoresis analysis. Every control experiment was performed on two distinct devices, each containing two sensors producing independent readouts. The same microfluidic operations were followed for both pre-PCR and post-PCR measurements; the sensor was functionalized with PLL and rinsed with buffer to achieve a steady baseline surface potential, then pressure was applied to flow the content of PCR channel over electronic sensors for 3 min, after which valves were closed and measurement buffer flow was restored. The PCR channel was replenished with starting PCR reagent as its content was flowed into the sensing channel. The greyed out area indicates the period of PCR channel injection, during which mechanical operations caused the sensor to lose its baseline value and drift temporarily. The higher and lower dotted segments are arbitrarily defined threshold levels for positive and negative signals, respectively.

subsequent closing) of microfluidic valves and the pressure fluctuations due to the injection of the PCR sample. However, when the valves were closed, and the initial measurement buffer flow condition was restored, the electronic reading became directly comparable to the initial baseline value again. While the sensors were also affected by transient conditions after thermocycling, the two distinct positive control experiments on different devices produced a permanent increase of more than 10 mV over baseline value, whereas the response from negative controls were less than 3.2 mV. To ensure that the sensor was functional after thermocycling and that the negative post-PCR measurements were not simply due to a loss in sensitivity, the sensors were subjected to a third measurement of 40 ng  $\mu\text{L}^{-1}$  50 bp ladder, which resulted in an approximately 9 mV response on all sensors. Based on the baseline shifts, a threshold value can be defined that converts the analog potential readings to a digital readout. For example, in this particular example, we defined 10 mV as a threshold for 'true' and 3.2 mV as a threshold for 'false'; a digital sequence detector would require a pre-PCR value of 'false' and post-PCR value of 'true' for a positive amplification.

The throughput of the device can be estimated by considering the time required for the individual steps followed in the experimental protocols. Before analysis of PCR product, the sensor requires a 2 h equilibration time following acid treatment. PCR requires approximately 1 h on a microdevice. Analysis of a single product requires 5 min for PLL-functionalization, which can occur at the same time as thermocycling, and another 5 min for DNA sensing. However, depending on the ultimate cost per device and specifics of the application, it may be more desirable to use the device in a disposable format where the sensor is equilibrated during the manufacturing process and packaged for immediate use.

## Conclusions

We have demonstrated a microsystem that integrates PCR and silicon field-effect sensors for label-free PCR detection. Using conventional PCR protocols, we showed the microsystem can reproducibly distinguish samples with and without the sequence of interest. While the system does not employ hybridization probes for an additional level of specificity, detection using polyelectrolyte multilayer assembly is a simple and direct way to measure a well-optimized standard PCR reaction, as it does not require additional steps or special PCR protocols to generate single stranded DNA for hybridization. We envision that by integrating additional functions such as sample purification and DNA extraction capabilities to the platform,<sup>48</sup> our approach could potentially be used for analysis of clinical and environmental samples.

## Acknowledgements

The authors thank Nebojsa Milovic, Scott Knudsen, Thomas Burg, and William Grover at Massachusetts Institute of Technology for helpful discussions. This work was supported by Air Force Office of Scientific Research, and Hewlett

Packard. C.H. acknowledges support from a MIT fellowship and the National Science Foundation Center for Bits and Atoms, and M.G. acknowledges support from Natural Sciences and Engineering Research Council of Canada (NSERC) through a post-doctoral fellowship. Devices were fabricated in the MIT Microsystems Technology Laboratories.

## References

- 1 R. K. Saiki, S. Scharf, F. Faloona, K. B. Mullis, G. T. Horn, H. A. Erlich and N. Arnheim, *Science*, 1985, **230**, 1350–1354.
- 2 M. Koudelka-Hep and P. D. van der Wal, *Electrochim. Acta*, 2000, **45**, 2437–2441.
- 3 R. H. Liu, J. Yang, R. Lenigk, J. Bonanno and P. Grodzinski, *Anal. Chem.*, 2004, **76**, 1824–1831.
- 4 A. T. Woolley and R. A. Mathies, *Proc. Natl. Acad. Sci. U. S. A.*, 1994, **91**, 11348–11352.
- 5 M. A. Burns, B. N. Johnson, S. N. Brahmasandra, K. Handique, J. R. Webster, M. Krishnan, T. S. Sammarco, P. M. Man, D. Jones, D. Heldsinger, C. H. Mastrangelo and D. T. Burke, *Science*, 1998, **282**, 484–487.
- 6 N. Zhang, H. Tan and E. S. Yeung, *Anal. Chem.*, 1999, **71**, 1138–1145.
- 7 M. A. Burns, C. H. Mastrangelo, T. S. Sammarco, F. P. Man, J. R. Webster, B. N. Johnson, B. Foerster, D. Jones, Y. Fields, A. R. Kaiser and D. T. Burke, *Proc. Natl. Acad. Sci. U. S. A.*, 1996, **93**, 5556–5561.
- 8 P. Belgrader, C. J. Elkin, S. B. Brown, S. N. Nasarabadi, G. D. Marshall, R. G. Langlois, F. P. Milanovich and B. W. Colston, *Anal. Chem.*, 2003, **75**, 3446–3450.
- 9 E. T. Lagally, C. A. Emrich and R. A. Mathies, *Lab Chip*, 2001, **1**, 102–107.
- 10 Y. K. Cho, J. Kim, Y. Lee, Y. A. Kim, K. Namkoong, H. Lim, K. W. Oh, S. Kim, J. Han, C. Park, Y. E. Pak, C. S. Ki, J. R. Choi, H. K. Myeong and C. Ko, *Biosens. Bioelectron.*, 2006, **21**, 2161–2169.
- 11 P. Belgrader, W. Benett, D. Hadley, G. Long, R. Mariella, Jr., F. Milanovich, S. Nasarabadi, W. Nelson, J. Richards and P. Stratton, *Clin. Chem.*, 1998, **44**, 2191–2194.
- 12 M. A. Northrup, B. Benett, D. Hadley, P. Landre, S. Lehw, J. Richards and P. Stratton, *Anal. Chem.*, 1998, **70**, 918–922.
- 13 C. S. Zhang, J. L. Xu, W. L. Ma and W. L. Zheng, *Biotechnol. Adv.*, 2006, **24**, 243–284.
- 14 J. Liu, M. Enzelberger and S. Quake, *Electrophoresis*, 2002, **23**, 1531–1536.
- 15 M. Krishnan, D. T. Burke and M. A. Burns, *Anal. Chem.*, 2004, **76**, 6588–6593.
- 16 A. Gulliksen, L. Solli, F. Karlsen, H. Rogne, E. Hovig, T. Nordstrom and R. Sirevag, *Anal. Chem.*, 2004, **76**, 9–14.
- 17 P. Belgrader, S. Young, B. Yuan, M. Primeau, L. A. Christel, F. Pourahmadi and M. A. Northrup, *Anal. Chem.*, 2001, **73**, 286–289.
- 18 N. C. Cady, S. Stelick, M. V. Kunnavakkam and C. A. Batt, *Sens. Actuators, B: Chemical*, 2005, **107**, 332–341.
- 19 J. A. Higgins, S. Nasarabadi, J. S. Karns, D. R. Shelton, M. Cooper, A. Gbakima and R. P. Koopman, *Biosens. Bioelectron.*, 2003, **18**, 1115–1123.
- 20 D. Baechi, R. Buser and J. Dual, *Sens. Actuators, A: Physical*, 2002, **95**, 77–83.
- 21 C. G. J. Schabmueller, J. R. Pollard, A. G. R. Evans, J. S. Wilkinson, G. Ensell and A. Brunnschweiler, *J. Micromech. Microeng.*, 2001, **11**, 329–333.
- 22 P. T. Monis, S. Giglio and C. P. Saint, *Anal. Biochem.*, 2005, **340**, 24–34.
- 23 K. Nath, J. W. Sarosy, J. Hahn and C. J. Di Como, *J. Biochem. Biophys. Methods*, 2000, **42**, 15–29.
- 24 O. Verhagen, M. J. Willemsse, W. B. Breunis, A. J. M. Wijkhuijs, D. C. H. Jacobs, S. A. Joosten, E. R. van Wering, J. J. M. van Dongen and C. E. van der Schoot, *Leukemia*, 2000, **14**, 1426–1435.
- 25 J. Fritz, E. B. Cooper, S. Gaudet, P. K. Sorger and S. R. Manalis, *Proc. Natl. Acad. Sci. U. S. A.*, 2002, **99**, 14142–14146.
- 26 J. Hahn and C. M. Lieber, *Nano Lett.*, 2004, **4**, 51–54.

- 
- 27 N. Milovic, M. J. Behr, R. M. Godin, J. Hou Chih-Sheng, R. Payer Kristofor, A. Chandrasekaran, R. Russo Peter, R. Sasisekharan and R. Manalis Scott, *Proc. Natl. Acad. Sci. U. S. A.*, 2006, **103**, 13374–13379.
- 28 A. Star, E. Tu, J. Niemann, J. C. P. Gabriel, C. S. Joiner and C. Valcke, *Proc. Natl. Acad. Sci. U. S. A.*, 2006, **103**, 921–926.
- 29 F. Uslu, S. Ingebrandt, D. Mayer, S. Bocker-Meffert, M. Odenthal and A. Offenhausser, *Biosens. Bioelectron.*, 2004, **19**, 1723–1731.
- 30 C.-S. J. Hou, N. Milovic, M. Godin, P. R. Russo, R. Chakrabarti and S. R. Manalis, *Anal. Chem.*, 2006, **78**, 2526–2531.
- 31 L. J. Kricka and P. Wilding, *Anal. Bioanal. Chem.*, 2003, **377**, 820–825.
- 32 M. A. Unger, H. P. Chou, T. Thorsen, A. Scherer and S. R. Quake, *Science*, 2000, **288**, 113–116.
- 33 E. B. Cooper, J. Fritz, G. Wiegand, P. Wagner and S. R. Manalis, *Appl. Phys. Lett.*, 2001, **79**, 3875–3877.
- 34 E. H. Nicollian and J. R. Brews, *MOS (metal oxide semiconductor) physics and technology*, Wiley-Interscience, New York, 1982.
- 35 J. Cheng, M. A. Shoffner, G. E. Hvichia, L. J. Kricka and P. Wilding, *Nucleic Acids Res.*, 1996, **24**, 380–385.
- 36 W. C. Dunn, S. C. Jacobson, L. C. Waters, N. Kroutchinina, J. Khandurina, R. S. Foote, M. J. Justice, L. J. Stubbs and J. M. Ramsey, *Anal. Biochem.*, 2000, **277**, 157–160.
- 37 B. C. Giordano, E. R. Copeland and J. P. Landers, *Electrophoresis*, 2001, **22**, 334–340.
- 38 J. N. Yang, Y. J. Liu, C. B. Rauch, R. L. Stevens, R. H. Liu, R. Lenigk and P. Grodzinski, *Lab Chip*, 2002, **2**, 179–187.
- 39 M. A. Shoffner, J. Cheng, G. E. Hvichia, L. J. Kricka and P. Wilding, *Nucleic Acids Res.*, 1996, **24**, 375–379.
- 40 B. Huang, H. K. Wu, S. Kim and R. N. Zare, *Lab Chip*, 2005, **5**, 1005–1007.
- 41 J. Goulpeau, D. Trouchet, A. Ajdari and P. Tabeling, *J. Appl. Phys.*, 2005, **98**.
- 42 A. Poghossian, A. Cherstvy, S. Ingebrandt, A. Offenhausser and M. J. Schoning, *Sens. Actuators, B: Chemical*, 2005, **111**, 470–480.
- 43 R. Y. Lai, E. T. Lagally, S. H. Lee, H. T. Soh, K. W. Plaxco and A. J. Heeger, *Proc. Natl. Acad. Sci. U. S. A.*, 2006, **103**, 4017–4021.
- 44 F. Lucarelli, G. Marrazza and M. Mascini, *Biosens. Bioelectron.*, 2005, **20**, 2001–2009.
- 45 G. Decher, *Science*, 1997, **277**, 1232–1237.
- 46 M. A. Innis and D. H. Gelfand, in *PCR applications: protocols for functional genomics*, ed. M. A. Innis, D. H. Gelfand and J. J. Sninsky, Academic Press, San Diego, 1990, pp. 3–13.
- 47 S. Cheng, C. Fockler, W. M. Barnes and R. Higuchi, *Proc. Natl. Acad. Sci. U. S. A.*, 1994, **91**, 5695–5699.
- 48 C. J. Easley, J. M. Karlinsey, J. M. Bienvenue, L. A. Legendre, M. G. Roper, S. H. Feldman, M. A. Hughes, E. L. Hewlett, T. J. Merkel, J. P. Ferrance and J. P. Landers, *Proc. Natl. Acad. Sci. U. S. A.*, 2006, **103**, 19272–19277.